LAWRENCE
LIVERMORE
NATIONAL
LABORATORY

LLNL-JRNL-575532

Turbulent ion heating from many overlapping laser beams in plasmas

P. Michel, W. Rozmus, E. A. Williams, L. Divol, R. L. Berger, R. P. J. Town, S. H. Glenzer, D. A. Callahan

August 21, 2012

Physical Review Letters

Turbulent ion heating from many overlapping laser beams in plasmas

P. Michel,[1] W. Rozmus,[2] E.A. Williams,[1] L. Divol,[1] R.L. Berger,[1] R.P.J. Town,[1] S.H. Glenzer,[1] and D.A. Callahan[1]

[1]*Lawrence Livermore National Laboratory, Livermore, CA 94551*

[2]*Theoretical Physics Institute, Department of Physics, University of Alberta, Alberta, Canada*

In this letter, we show through numerical simulations and analytical results that overlapping multiple (N) laser beams in plasmas can lead to strong turbulent ion heating from many ($\propto N^2$) electrostatic perturbations driven by beat waves between pairs of laser beams. For typical inertial confinement fusion experiments conditions, hundreds of such beat waves are driven in mm^3-scale plasmas, leading to ion heating rates of several keVs/ns. This mechanism has important consequences for the saturation of cross-beam energy transfer and the overall hydrodynamics evolution of such laser-plasma systems.

Experiments on large scale laser facilities exploring High Energy Density Physics (HEDP) or Inertial Confinement Fusion (ICF) often require overlapping multiple intense ($> 10^{14}\,W/cm^2$) laser beams in plasmas [1–3]. This leads to a wide range of new and complex multi-beam laser-plasma interaction phenomena such as cross-beam energy transfer (CBET) [4], which plays a crucial role for both the indirect-drive and direct-drive approaches to ICF. On indirect-drive experiments at the National Ignition Facility (NIF), CBET is used at an advantage via laser wavelengths adjustments to tune the ICF targets' implosion symmetry [5–7]. On the other hand, for direct-drive experiments at the Omega facility, CBET tends to reduce the laser energy absorbed in the corona and is mitigated by adjusting the laser beams' radii [8, 9]. In such situations, the overlap of N laser beams generates $N(N-1)/2$ individual beat waves whose phase velocities are fixed (determined by the laser beams' wavelengths and directions), and can be near the ion acoustic velocity due to either small wavelength adjustments as is done on NIF (cf. Fig. 1), or to sonic flows as in direct-drive experiments. Each beat wave drives an electrostatic potential via the ponderomotive force, with a resulting density perturbation which is largest as the beat wave's phase velocity approaches the ion acoustic velocity. The scattering of laser light on these driven fluctuations can transfer momentum and energy to the plasma: for each photon scattered from laser beam n to laser beam m, the momentum and energy transferred are respectively $\delta \boldsymbol{p} = \hbar(\boldsymbol{k}_n - \boldsymbol{k}_m)$ and $\delta U = \hbar(\omega_n - \omega_m)$, where $\omega_{m,n}$ and $\boldsymbol{k}_{m,n}$ are the photons' frequencies and wave vectors. Thus, overlapping many of these driven waves can in principle affect the hydrodynamics evolution.

In this letter, we show that the interactions of many beat waves with a plasma can lead to strong turbulent heating of the ions and modify the local hydrodynamic conditions where multiple laser beams overlap. This can in turn strongly modify the laser-plasma interaction mechanisms that take place in such regions, such as CBET. Using a particle code including binary collisions, we show that the beat waves create an energetic tail in the ion distribution function over time scales of a few ion bounce periods. Then, on time scales longer than the ion-ion collision time, collisions transfer the energy from the hot tail into the bulk; the distribution recovers a nearly-Maxwellian shape, but with a rapidly-increasing temperature and a change in average (flow) velocity. For typical NIF conditions, we calculate ion heating rates of several keVs/ns, which also leads to a $\simeq$50% increase of the ion acoustic velocity in less than a nanosecond. The ion heating process can in turn saturate CBET; for similar NIF conditions, we calculate a reduction of CBET linear gains by $\sim$4-5$\times$. The process eventually stabilizes as the ion acoustic velocity becomes larger than the drivers' phase velocities.

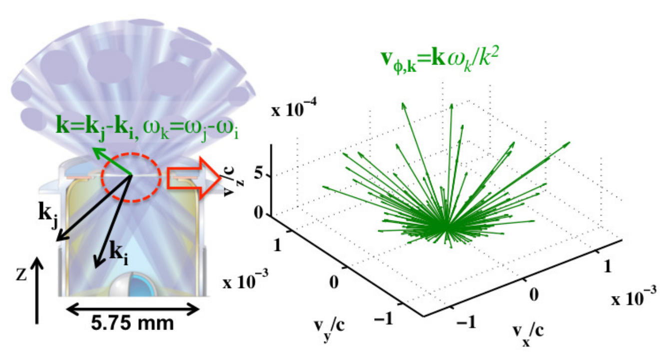

FIG. 1: Schematic view of a NIF hohlraum laser entrance hole; 24 quadruplets of laser beams overlap in a mm^3-scale plasma at each laser entrance hole, leading to 276 possible individual pairs. Each pair of quads (m, n) drives a beat wave with a phase velocity $\boldsymbol{v}_{\phi,k} = \boldsymbol{k}\omega_k/k^2$, where $\omega_k = \omega_n - \omega_m$ and $\boldsymbol{k} = \boldsymbol{k}_n - \boldsymbol{k}_m$. The beat waves' $\boldsymbol{v}_{\phi,k}$ are represented on the right (green arrows), for a wavelength separation between inner and outer beams of $\Delta\lambda$=2 Å (defined at the laser wavelength on target, $\lambda_0 \simeq$351 nm).

Our numerical model calculates the ion distribution function $f_i(\boldsymbol{r}, \boldsymbol{v}, t)$ by integrating equations of motion of particles in the presence of many beat waves and collisions; the resulting space-averaged particle distribution function is then used to calculate the self-consistent evolution of the fields. Each beat wave between two lasers (m, n) with frequencies $\omega_{m,n}$ and wave vectors $\boldsymbol{k}_{m,n}$ creates a ponderomotive potential $\phi_{p,k} = \frac{1}{2}\hat{\phi}_{p,k}\exp[i\psi_k] +$

c.c. oscillating at the beat wave's phase, $\psi_k = \boldsymbol{k}\cdot\boldsymbol{r} - \omega_k t + \nu_k$, where $\omega_k = \omega_n - \omega_m$, $\boldsymbol{k} = \boldsymbol{k}_n - \boldsymbol{k}_m$ and ν_k is a random phase term between 0 and 2π which accounts for the fact that laser beams on large scale facilities are typically optically smoothed and thus uncorrelated with one-another. Beat waves from two laser beams with different frequencies ($\omega_k \neq 0$) have a finite phase velocity $\boldsymbol{v}_{\phi,k} = \boldsymbol{k}\omega_k/k^2$. The ponderomotive potential acts on the electrons to create a charge separation which results in an electrostatic potential $\phi_k = \frac{1}{2}\hat{\phi}_k \exp[i\psi_k] + c.c.$ which acts on both the electrons and the ions. The equations of motion for the ions are integrated with a Runge Kutta method in the presence of many of these electrostatic potentials and with ion-ion collisions, $M_i d\boldsymbol{v}_i/dt = -q_i \sum_k \boldsymbol{\nabla}\phi_k(\boldsymbol{r},t) + \bar{C}_{i-i}$, where M_i and q_i are the ion mass and charge, and $\bar{C}_{i-i}$ is a binary ion-ion collision operator based on the scheme from Takizuka and Abe [10]. Here we assume that the electrons response is linear and that their averaged distribution remains Maxwellian with a constant temperature. As will be discussed later, only ion-ion collisions will be significant for ICF-relevant conditions; electron-ion thermal equilibration rates are typically too slow for the ions to affect the electron temperature.

The resulting ion distribution function is used to self-consistently calculate the evolution of the electrostatic potentials. The main assumption of the model is that these potentials have spatially uniform, slowly time-varying envelopes, $\hat{\phi}_k = \hat{\phi}_k(t)$, and follow the time-evolution of the spatially averaged distribution function. Wave-wave couplings are neglected. The ion distribution is thus decomposed into its spatial average and the responses to the waves, $f_i(\boldsymbol{r},\boldsymbol{v},t) = f_{i0}(\boldsymbol{v},t) + \sum_k \delta f_{ik}(\boldsymbol{r},\boldsymbol{v},t)$, where f_{i0} varies slowly compared to the fast oscillations of the beat waves. Poisson's equation connects each beat wave's electrostatic potential to the resulting density perturbation: $-\nabla^2\phi_k = 4\pi \sum_\alpha \int d^3v \delta f_{\alpha k}$ where α is the particle specie ($= e$ or i). Combining it with Vlasov equation, $[\partial_t + \boldsymbol{v}\cdot\boldsymbol{\nabla} - (q_\alpha/m_\alpha)\sum_k \boldsymbol{\nabla}(\phi_k + \delta_{e\alpha}\phi_{p,k})\partial_{\boldsymbol{v}}]f_\alpha = 0$, where $\delta_{\alpha\alpha'}$ is a Kronecker delta, we get the expression for the electrostatic potential driven by the ponderomotive potential: $(1+\chi_{ek}+\chi_{ik})\hat{\phi}_k = -\chi_{ek}\hat{\phi}_{p,k}$. For hot plasmas ($\geq 1$ keV), the phase velocities are negligible compared to the electron thermal velocity, $v_{\phi,k} \ll v_{Te}$, so the electron susceptibility is $\chi_{ek} \simeq 1/(k\lambda_{De})^2$ (calculations with electrons showed no changes in their distribution function; in the following we will thus only consider the evolution of the ion distribution). On the other hand, the beat waves' phase velocities can be of the same order as (or larger than) the ion thermal velocity. The ion susceptibility evolution follows the space-averaged ion distribution:

$$\chi_{ik}(t) \;=\; \frac{4\pi q_i^2}{k^2 m_i}\int \boldsymbol{k}\cdot\frac{\partial f_{i0}(\boldsymbol{v},t)}{\partial\boldsymbol{v}}\frac{d^3v}{\omega - \boldsymbol{k}\cdot\boldsymbol{v}}. \qquad (1)$$

The amplitudes of the electrostatic potentials thus follow the slowly-varying space-averaged distribution function f_{i0},with:

$$\phi_k(\boldsymbol{r},t) = |\hat{\phi}_{p,k}|\frac{\chi_{ek}}{|1+\chi_{ek}+\chi_{ik}(t)|}\cos[\psi_k(\boldsymbol{r},t)]. \qquad (2)$$

The integration in Eq. (1) is carried out numerically similarly to Ref. [11]. The expression for each ponderomotive potential $\phi_{p,k}$ created by two laser beams (m,n) with circular polarizations (or, equivalently, two NIF quads with polarization smoothing) crossing at an angle θ_{mn} is $|\hat{\phi}_{p,k}| = \frac{1}{4}(m_e c^2/e)a_m a_n(1+\cos^2\theta_{mn})^{1/2}$, where $a = v_{osc}/c \approx 0.85(I_{18}\lambda_\mu^2)^{1/2}$ is the normalized laser vector potential (I_{18} is the laser intensity in units of $10^{18}\,W/cm^2$ and λ_μ its wavelength in microns). In the case of two beams with parallel polarizations, we have $|\hat{\phi}_{p,k}| = \frac{1}{2}(m_e c^2/e)a_m a_n$.

We present calculations for the entrance hole of a NIF hohlraum, where 24 quadruplets or "quads" of laser beams cross, generating 276 beat waves overlapping in a mm^3-scale plasma (cf. Fig. 1). The quads are grouped in four cones propagating at 23.5° (4 quads), 30° (4 quads), 44.5° (8 quads) and 50° (8 quads) from the hohlraum axis; the "inner quads" (23.5° and 30°) have an average intensity of $5\times10^{14}\,W/cm^2$ and the "outer quads" (44.5° and 50°) are at $10^{15}\,W/cm^2$. The initial electron and ion temperatures are 2.8 and 0.8 keV respectively, the electron density is 3% of critical, and the plasma is He (Z=2); these are typical conditions at the beginning of the main ("fourth") NIF laser pulse. The 128 beat waves between an inner and an outer quad have a finite phase velocity, set by a wavelength shift of 2 Å (at λ_0=351 nm) between inner and outer quads [5, 12]. The 148 others, generated by pairs of laser beams with similar wavelengths, are stationary in the laboratory frame, v_ϕ=0. For these conditions, the ion-ion collision time is $\tau_{ii} \simeq$60 ps. On the other hand, the thermal equilibration time for the electrons is $\tau^{e|i} \simeq 6$ ns [13]; this is too slow to be relevant for our conditions and is why we only consider ion-ion collisions in our model.

The evolution of the ion distribution function is shown on Fig. 2 for typical NIF conditions. The 276 green dots represent the beat waves' phase velocities. Due to the NIF geometry, the problem is axisymmetric around z, the hohlraum axis (cf. Fig. 1). The ion distribution is initially Maxwellian at t=0. Some of the beat waves have their phase velocities near the acoustic velocity c_s, which is represented as a cyan iso-contour line. These beat waves drive the strongest electrostatic perturbations. Overall, the initial electrostatic potentials amplitudes $\hat{\phi}_k$ are in the range $[10^{-6}-10^{-5}]\,m_e c^2/e$, corresponding to density perturbations $\delta n/n \approx [10^{-4}-10^{-3}]$. The ion bounce periods τ_b are of a few ps.

In the early stages, for times smaller than the collision time (t$\leq \tau_{ii} \simeq$60 ps), some potentials $\hat{\phi}_k(t)$ exhibit nonlinear oscillations at τ_b due to trapped particles, similarly to Ref. [14]. However, after a few bounce periods, turbulence starts to dominate, diffusing particles between

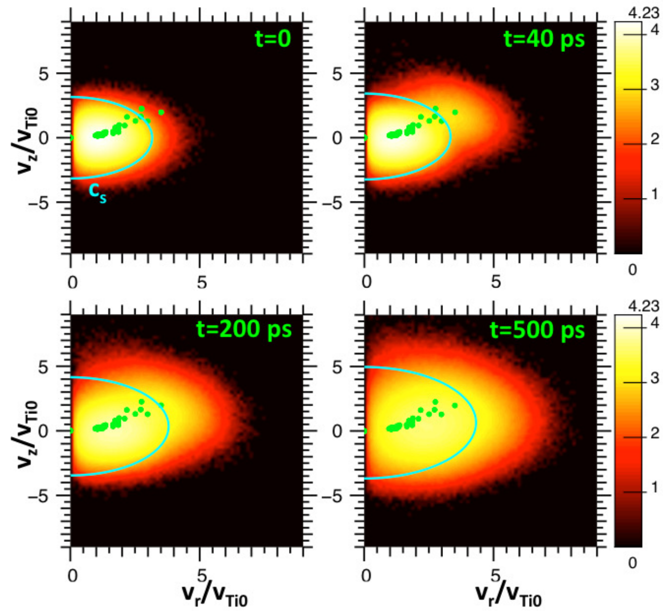

FIG. 2: Ion velocity distribution function $\log[f_i(\boldsymbol{v})]$, plotted vs. v_z and v_r (the distribution is axisymmetric along z) at times t=0, 40, 200 and 500 ps. The cyan contour line represents the ion acoustic velocity c_s, and the green dots represent the 276 electrostatic drivers for the NIF geometry with $\Delta\lambda$=6 Å. The initial plasma conditions are T_e=2.8 keV, T_i=0.8 keV, n_e/n_c=3% and Z=2 (He), and the laser beams intensities are 5×10^{14} and 10^{15} W/cm^2 for the "inner" and "outer" beams, respectively. These are typical conditions at the laser entrance holes of a NIF hohlraum during the early part of the main laser pulse.

multiple overlapping resonances. The non-linear oscillations disappear, and an energetic tail starts to develop in the ion distribution near the velocity of the fastest drivers, around 3 to 4 times the initial ion thermal velocity v_{Ti0}, as is shown in Fig. 2 at t=40 ps. At this stage, the electrostatic potentials exhibit a complex evolution; the distortion of the distribution function can either decrease or increase their amplitudes, and overall, the trend is generally upwards. The total kinetic energy of the particles rapidly increases due to continuous injection of ions into the hot tail.

At later times, for $t \gg \tau_{ii}$, ion-ion collisions restore the energy from the hot tail back into the bulk, leading to an increase in ion temperature. After 200 ps, the bulk of ions has broadened and reached a thermal velocity close to the phase velocity of the fastest drivers; the tail that was present at t=40 ps is now barely visible. At t=500 ps, the distribution resembles a drifting Maxwellian.

The thermal energy of the particles and their average velocity are shown in Fig. 3a-b. The ion temperature increases up to 4 keV in less than a nanosecond, and the particles acquire a drift $\langle v_z\rangle$ of about 10^7 cm/s due to momentum deposition [15]. The acoustic velocity $c_s = [(Zk_BT_e + 3k_BT_i)/M_i]^{1/2}$ increases from 4.4×10^7 cm/s to 6.7×10^7 cm/s in 1 ns.

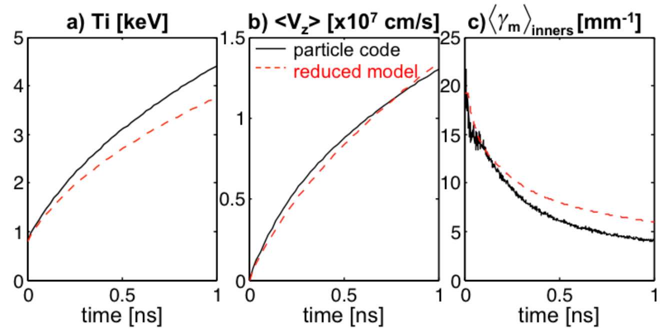

FIG. 3: Time evolution of: a) ion temperature (defined as $kT_i = \frac{1}{3}M_i(\langle v^2\rangle - \langle v\rangle^2)$), b) average velocity, and c) the average exponential CBET spatial gain for a NIF inner beam. The black curves are the results from the code, and the dashed red are from the quasi-linear reduced model described in the text.

Such ion heating rates are in qualitative agreement with simple estimates based on the conservation of action [16] during the CBET process, using experimental measurements. Typically, symmetric implosions on NIF for 420 TW shots require transferring 100-150 TW between laser beams in a $\simeq$mm^3-size plasma near the hohlraum's laser entrance holes. The power density deposited into plasma waves is therefore [100-150] TW$\times\delta\lambda/\lambda_0 \simeq 60$ to 120 GW/mm^3 for wavelength separations between laser beams of 2-3 Å (and λ_0=351 nm). Assuming an average ion density $n_i = 1.35\times10^{20}$ cm^{-3}, and that all the waves energy eventually gets converted into heat, we get ion heating rates of 2-5 keVs/ns.

Since the volume where all the beams overlap is of the order of a mm^3, the flow (similar to a Mach 1 nozzle flow near the entrance hole) will totally replace the ion population in that volume in 2-3 ns; the other hydrodynamics conditions will also change, which is why we limit our calculations to 1 ns.

The effect of ion heating on CBET is represented in Fig. 3c, which shows the average spatial gain exponent for the NIF "inner beams". The gain is defined using the convective growth formula for beam m from beam n [12, 15]:

$$\partial_z a_m^2 = -\frac{\chi_{ek}^2 \mathrm{Im}(\chi_{ik})}{|1+\chi_{ek}+\chi_{ik}|^2}\frac{k^2}{16k_m}a_m^2 a_n^2\left[1+\cos^2(\theta_{mn})\right]. \quad (3)$$

Fig. 3c represents the average over all NIF's "inner beams" of the linearized gain on intensities γ_m such that $a_m^2(z+\delta z) \approx a_m^2(z)\exp[\gamma_m\delta z]$.

The gain drops by a factor $\sim 4-5$, which could help explain the observed saturation of CBET in both direct- and indirect-drive experiments despite very low levels of density fluctuations [8, 17, 18].

The heating rate eventually drops: the temperature increases up to the point where the acoustic velocity (cyan iso-contour on Fig. 2) reaches the largest drivers' phase velocities (soon after t=200 ps in our simulations). From then on, the ion acoustic resonance will be moved further away from the beat waves' fixed phase velocities, which will rapidly reduce their coupling to the plasma and thus rapidly slow down the ion heating. This also means that the plasma will set itself back into a regime where the individual waves responses are essentially linear, by pushing the resonance away from the waves.

Since collisions tend to rapidly thermalize the hot ion tail and restore a Maxwellian shape for the distribution function, we can derive a simple reduced model based on the assumption that the distribution remains Maxwellian at all times, but with a time-varying temperature and average velocity. The time-evolution of the average velocity and temperature can be derived from the space-averaged distribution f_{i0}, following quasi-linear theory [19–21]. The distribution follows a quasi-linear diffusion equation: $\partial_t f_0(\boldsymbol{v},t) = \partial_{\boldsymbol{v}} \cdot \bar{D} \cdot \partial_{\boldsymbol{v}} f_0(\boldsymbol{v},t)$, with the following quasi-linear operator:

$$\bar{D} = \frac{q_i^2}{2M_i^2} \sum_k |\hat{\phi}_k|^2 \boldsymbol{k}\boldsymbol{k} \mathrm{Im} \frac{1}{\omega_k - \boldsymbol{k}\cdot\boldsymbol{v}}. \tag{4}$$

By taking the moments of f_{i0}, one can calculate the average flow and thermal energy, $\langle \boldsymbol{v} \rangle = n_i^{-1} \int d^3 v \boldsymbol{v} f_{i0}(\boldsymbol{v},t)$ and $k_B T_i = \frac{1}{3} M_i (\langle v^2 \rangle - \langle v \rangle^2)$. Both are coupled via the time-varying ion susceptibility χ_i, so we get the following system of coupled equations:

$$\begin{aligned} \frac{d\langle \boldsymbol{v} \rangle}{dt} &= \frac{-1}{8\pi M_i n_i} \sum_k |\hat{\phi}_k|^2 k^2 \mathrm{Im}(\chi_{ik}) \boldsymbol{k}, & (5) \\ \frac{dk_B T_i}{dt} &= \frac{1}{12\pi n_i} \sum_k |\hat{\phi}_k|^2 k^2 \left(\omega_k - \boldsymbol{k}\cdot\langle \boldsymbol{v} \rangle\right) \mathrm{Im}(\chi_{ik}), & (6) \\ \chi_{ik}(t) &= \frac{-\omega_{pi}^2 m_i}{2k^2 k_B T_i} Z' \left[\frac{\omega_k - \boldsymbol{k}\cdot\langle \boldsymbol{v} \rangle}{k\sqrt{2k_B T_i/m_i}} \right], & (7) \end{aligned}$$

where Z' is the plasma dispersion function. Eq. (5) is similar to that of Williams et al. [15] if ϕ_{pk} is estimated for the case of laser beams with parallel polarizations.

The total energy of the ions $U_{tot} = \frac{1}{2} M_i \langle v^2 \rangle$ is distributed between thermal and flow energy, $U_{tot} = \frac{3}{2} k_B T_i + U_{flow}$ where $U_{flow} = \frac{1}{2} M_i \langle v \rangle^2$. Note that for beat waves from lasers with identical frequency, i.e. $\omega_k = 0$, there is no net transfer of energy to the plasma since $dU_{tot}/dt = 0$ per Eqs. (5)-(6); there is however a redistribution of the total energy of the ions from flow energy to heat. The implication is that even for configurations where all the laser beams have the same wavelength, if beams cross in a flowing plasma they will not only exchange energy [22], but will also reduce the plasma flow and increase the ion temperature.

This reduced model is compared to our particle code in Fig. 3. Because ion-ion collisions thermalize the distribution quickly enough, this simple model reproduces the code's result to better than 20% for the temperature and CBET gains, and to a few % for the momentum. The disagreement for T_i comes from the fact that the distribution from the particle code still maintains a slight tail even at later times when $t \gg \tau_{ii}$. The agreement is better for the momentum which is only the first order moment of f_{i0} and is less sensitive to variations in the detailed shape of the distribution function. This simple model could in principle be included in hydrodynamics codes without major impact on the computation time. This would improve the description of the hydrodynamics conditions in regions where many laser beams overlap, and would also reduce the self-consistently calculated CBET linear gains.

Turbulent ion heating could also modify other laser-plasma interaction processes occurring in regions where many laser beams overlap, such as the re-amplification of backscatter light generated by a single laser beam inside a NIF target by all the other incoming laser beams crossing the backscatter wave on its way out [23].

In conclusion, we have shown that strong ion heating can occur when multiple laser beams overlap in plasmas. The numerous beat waves between pairs of crossing laser beams drive electrostatic perturbations which can transfer energy and momentum to the ions, leading to turbulent heating and plasma drift. For typical NIF conditions, the ion temperature can be increased at rates of several keVs/ns. This in turn saturates the cross-beam energy transfer process, with a drop in linear gains by 4-5× in less than a nanosecond. A simple quasi-linear model is shown to reproduce the main observables from the particle code. The heating rate eventually slows down as the increase in ion acoustic velocity pushes the ion acoustic resonance away from the laser-driven beat waves. One could envision using controlled CBET to locally heat the plasma and mitigate other laser-plasma interaction processes.

Acknowledgments

This work was performed under the auspices of the U.S. Department of Energy by Lawrence Livermore National Laboratory under Contract DE-AC52-07NA27344.

[1] J. D. Lindl, P. Amendt, R. L. Berger, S. G. Glendinning, S. H. Glenzer, S. W. Haan, R. L. Kauffman, O. L. Landen, and L. J. Suter, Phys. Plasmas **11**, 339 (2004).

[2] N. Fleurot, C. Cavailler, and J. L. Bourgade, Fusion En-

gineering and Design **74**, 147 (2005).

[3] R. L. McCrory, D. D. Meyerhofer, R. Betti, R. S. Craxton, J. A. Delettrez, D. H. Edgell, V. Y. Glebov, V. N. Goncharov, D. R. Harding, D. W. Jacobs-Perkins, et al., Physics of Plasmas **15**, 055503 (pages 8) (2008).

[4] W. L. Kruer, S. C. Wilks, B. B. Afeyan, and R. K. Kirkwood, Phys. Plasmas **3**, 382 (1996).

[5] P. Michel, L. Divol, E. A. Williams, S. Weber, C. A. Thomas, D. A. Callahan, S. W. Haan, J. D. Salmonson, S. Dixit, D. E. Hinkel, et al., Phys. Rev. Lett. **102**, 025004 (2009).

[6] S. H. Glenzer, B. J. MacGowan, P. Michel, N. B. Meezan, L. J. Suter, S. N. Dixit, J. L. Kline, G. A. Kyrala, D. K. Bradley, D. A. Callahan, et al., Science **327**, 1228 (2010).

[7] J. D. Moody, P. Michel, L. Divol, R. L. Berger, E. Bond, D. K. Bradley, D. A. Callahan, E. L. Dewald, S. Dixit, M. J. Edwards, et al., Nature Phys. **8**, 344 (2012).

[8] I. V. Igumenshchev, W. Seka, D. H. Edgell, D. T. Michel, D. H. Froula, V. N. Goncharov, R. S. Craxton, L. Divol, R. Epstein, R. Follett, et al., Physics of Plasmas **19**, 056314 (2012).

[9] D. H. Froula, I. V. Igumenshchev, D. T. Michel, D. H. Edgell, R. Follett, V. Y. Glebov, V. N. Goncharov, J. Kwiatkowski, F. J. Marshall, P. B. Radha, et al., Phys. Rev. Lett. **108**, 125003 (2012).

[10] T. Takizuka and H. Abe, Journal of Computational Physics **25**, 205 (1977), ISSN 0021-9991.

[11] J. P. Palastro, J. S. Ross, B. Pollock, L. Divol, D. H. Froula, and S. H. Glenzer, Phys. Rev. E **81**, 036411 (2010).

[12] P. Michel, S. H. Glenzer, L. Divol, D. K. Bradley, D. Callahan, S. Dixit, S. Glenn, D. Hinkel, R. K. Kirkwood, J. L. Kline, et al., Phys. Plasmas **17**, 056305 (2010).

[13] J. D. Huba, *NRL Plasma Formulary*, Naval Research Laboratory, Washington, D.C. (2006).

[14] T. O'Neil, Physics of Fluids **8**, 2255 (1965).

[15] E. A. Williams, B. I. Cohen, L. Divol, M. R. Dorr, J. A. Hittinger, D. E. Hinkel, A. B. Langdon, R. K. Kirkwood, D. H. Froula, and S. H. Glenzer, Phys. Plasmas **11**, 231 (2004).

[16] J. Manley and H. Rowe, Proceedings of the IRE **44**, 904 (1956), ISSN 0096-8390.

[17] I. V. Igumenshchev, D. H. Edgell, V. N. Goncharov, J. A. Delettrez, A. V. Maximov, J. F. Myatt, W. Seka, A. Shvydky, S. Skupsky, and C. Stoeckl, Physics of Plasmas **17**, 122708 (pages 5) (2010).

[18] P. Michel, L. Divol, R. P. J. Town, M. D. Rosen, D. A. Callahan, N. B. Meezan, M. B. Schneider, G. A. Kyrala, J. D. Moody, E. L. Dewald, et al., Phys. Rev. E **83**, 046409 (2011).

[19] W. E. Drummond and D. Pines, Nucl. Fusion Suppl. **3**, 1049 (1962).

[20] A. A. Vedenov, E. P. Velikhov, and R. Z. Sagdeev, Nucl. Fusion **1**, 82 (1961).

[21] I. B. Bernstein and F. Engelmann, Physics of Fluids **9**, 937 (1966).

[22] R. K. Kirkwood, J. D. Moody, A. B. Langdon, B. I. Cohen, E. A. Williams, M. R. Dorr, J. A. Hittinger, R. Berger, P. E. Young, L. J. Suter, et al., Phys. Rev. Lett. **89**, 215003 (2002).

[23] R. K. Kirkwood, P. Michel, R. London, J. D. Moody, E. Dewald, L. Yin, J. Kline, D. Hinkel, D. Callahan, N. Meezan, et al., Physics of Plasmas **18**, 056311 (2011).